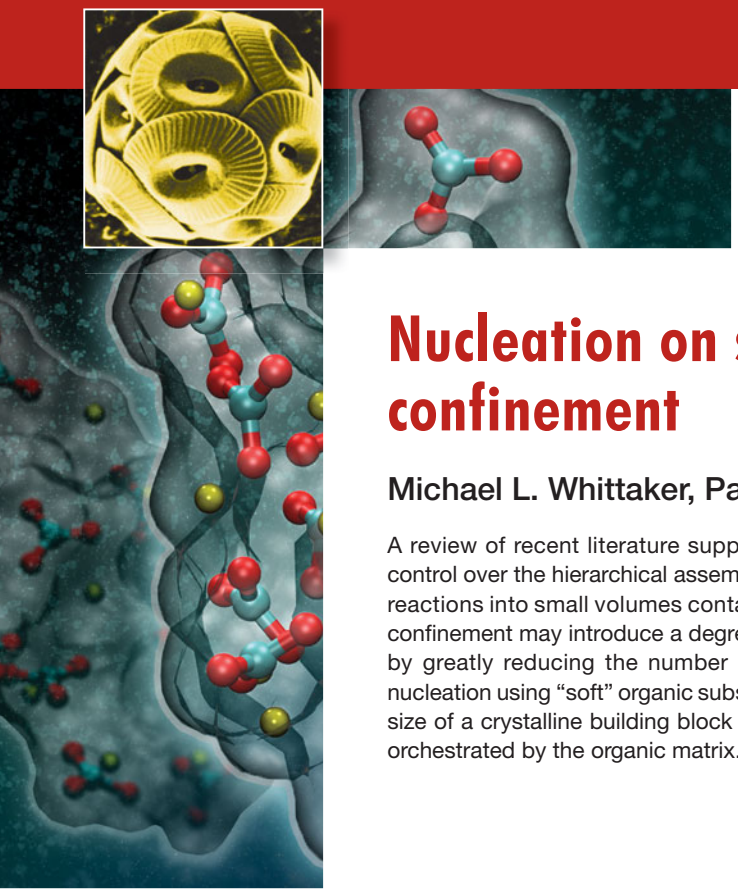


Nucleation on surfaces and in confinement

Michael L. Whittaker, Patricia M. Dove, and Derk Joester

A review of recent literature supports the notion that organisms may achieve nanoscale control over the hierarchical assembly of organic–inorganic materials by compartmentalizing reactions into small volumes containing specifically functionalized macromolecules. Such confinement may introduce a degree of determinism to the stochastic process of nucleation by greatly reducing the number of nucleation events, allowing an organism to control nucleation using "soft" organic substrates. In this way, the polymorph, orientation, shape, and size of a crystalline building block can be selected, and its assembly into a larger structure orchestrated by the organic matrix.

Introduction

Mineralized tissues support locomotion (e.g., bones), predation (teeth), and defense (shells), and are used for sensing acceleration (e.g., vertebrate otoliths and otoconia), gravity (statoliths), light (lenses), and magnetic fields (magnetosomes), often doubling as nutrient/waste storage.[1] Many of their remarkable properties emerge from the hierarchical organization of organic and inorganic building blocks (**Figure 1**)[2–7] (also see the June 2015 *MRS Bulletin* issue: *Biomineralization*). Despite new experimental techniques[8–12] and continuous improvements in computational approaches,[13,14] we are still far from understanding how the organisms direct mineral nucleation and subsequent processes that lead to assembly.[15–17] This article focuses on our current understanding of two critical aspects of biomineralization—(1) how self-assembled surfaces direct location, orientation, and timing through heterogeneous nucleation; and (2) the effect of confinement within small volumes on the rate of phase transformations.

A brief review of nucleation in biomineralization

Biomineralization typically starts with precipitation from a supersaturated aqueous solution.[16,18] The driving force for the formation of a new phase with the chemical formula $[(A_1)_{k_1}(A_2)_{k_2}\ldots(A_i)_{k_i}]$ can be expressed in terms of the supersaturation:

$$\sigma = \ln\left[\frac{\prod_i [A_i]^{k_i}}{K_{sp}}\right], \quad (1)$$

where K_{sp} is the solubility product of the new phase, $[A_i]$ refers to the activity of the aquo-complex of the i^{th} species (A_i) in solution, and k_i is the associated stoichiometric coefficient. Clusters of the new phase arise from concentration fluctuations. According to classical nucleation theory (CNT), a cluster that is exactly of critical size, the nucleus, is in unstable equilibrium, and either loss or gain of additional building blocks will reduce its free energy. Smaller clusters will on average shrink, and larger ones will grow. The reversible work of nucleation W^* is the free-energy cost (barrier) associated with the formation of a spherical, incompressible nucleus:

$$W^* = \frac{16\pi}{3}\left(\frac{V_m}{RT}\right)^2 \frac{\gamma^3}{\sigma^2}, \quad (2)$$

where γ is the (average) surface free energy of the newly formed interface, R is the universal gas constant, T is temperature, and V_M is the molar volume of the new phase.[19] As discussed in the article by Sear in this issue, the intrinsic nucleation rate J_V, the number of nuclei formed per unit time and unit volume, then takes the form:[20]

$$J_V \propto e^{-\frac{W^*}{k_B T}}, \quad (3)$$

where k_B is the Boltzmann constant.

Michael L. Whittaker, Department of Materials Science and Engineering, Northwestern University, USA; m.whittaker@u.northwestern.edu
Patricia M. Dove, Department of Geosciences, Virginia Polytechnic Institute and State University, USA; pdove@vt.edu
Derk Joester, Department of Materials Science and Engineering, Northwestern University, USA; d-joester@northwestern.edu
doi:10.1557/mrs.2016.90

© 2016 Materials Research Society
https://doi.org/10.1557/mrs.2016.90 Published online by Cambridge University Press

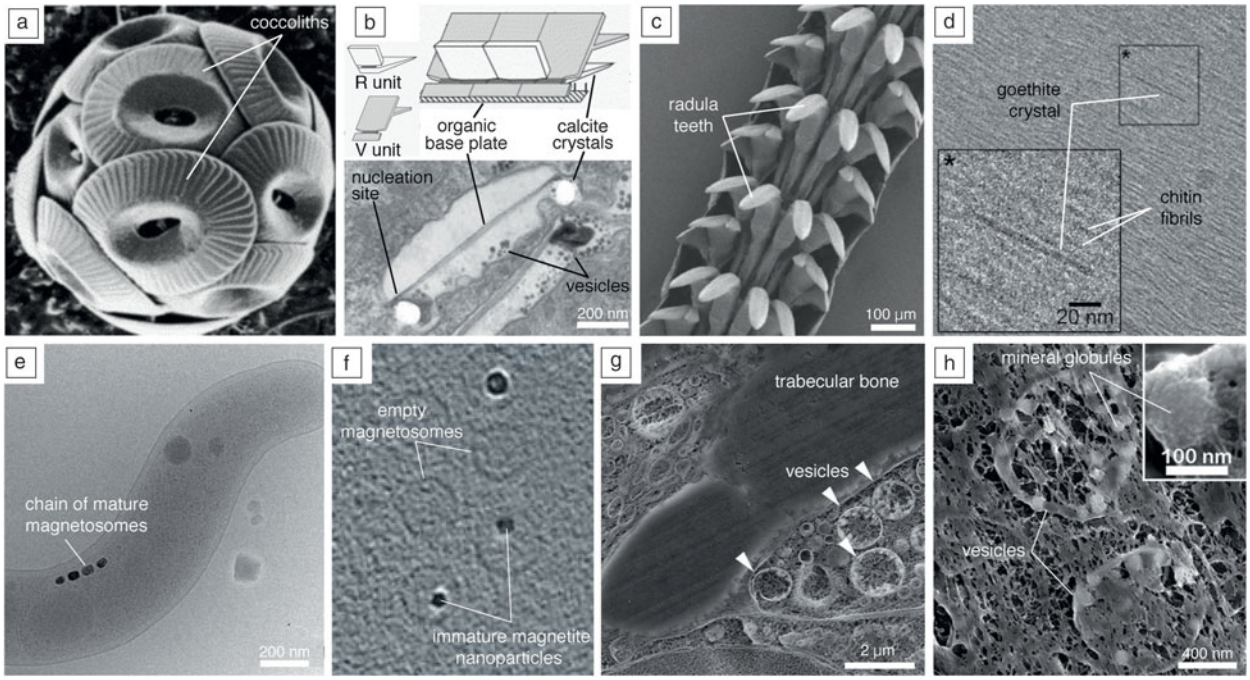


Figure 1. Heterogeneous nucleation and confinement in biomineralization. (a) Coccoliths are elements of the extracellular coccosphere in coccolithophores, a class of unicellular marine algae. Heterococcoliths (labeled coccoliths) are composed of a ring of elaborately shaped calcite ($CaCO_3$) single crystals attached to an organic base plate. (b) Coccoliths are composed of alternating, interdigitated R and V units that differ in shape and crystallographic orientation. Precipitation is confined within vesicles inside the cell and involves heterogeneous, oriented nucleation in specific locations along the periphery of the baseplate.[2,3] (c–d) Limpets are intertidal mollusks that graze on rocks using (c) exceptionally hard, iron oxide-based radula teeth. (d) During mineralization, goethite crystals nucleate on a preformed matrix of chitin fibers.[4] Inset is a high-magnification image of the black box. (e–f) In magnetotactic bacteria, (e) magnetite nanoparticles are confined within magnetosome vesicles, (f) allowing for alignment and navigation in magnetic fields.[5,6] (g–h) Calcium phosphate mineral precipitates (labeled mineral globules) in intracellular vesicles observed in neonatal mouse calvaria, a model for human bone mineralization.[7] Inset is a high-magnification image of a mineral globule.

In the presence of any heterogeneities in the parent phase (heterogeneous nucleators), the height of the barrier is reduced by a structure factor, S, which depends upon the specific geometry of the nucleus and interface between the nucleus and the nucleator.[21] Alternatively, the impact of heterogeneous nucleators can be expressed by assigning a net effective surface free energy, γ_{net}:[22,23]

$$J_V^{het} \propto e^{-\frac{W^*}{k_B T}S} = e^{-f\left\{\frac{V_m}{RT}\right\}^2 \frac{\gamma_{net}^3}{\sigma^2}}. \quad (4)$$

The nucleation rate is extremely sensitive to the presence of heterogeneous nucleators, about which little is known in bulk experiments. Consequently, determination of γ from nucleation rate data is difficult, and a wide range of values have been reported (i.e., calcite [64–1480 mJ/m^2]).[24–27] Similar to other crystalline solids, nucleation at moderate supersaturation is expected to proceed extremely slowly when heterogeneous nucleators are absent.[24,25] Metastable amorphous calcium carbonate (ACC), however, forms readily under similar conditions. While ACC is frequently observed *in vivo* and *in vitro*, the mechanism of its formation and subsequent transformation into one of the crystalline polymorphs of calcium carbonate remains the topic of much debate.[13,28]

Nucleation on surfaces

Irrespective of whether a metastable phase such as ACC precedes the formation of a biomineral, the onset of mineralization likely involves heterogeneous nucleators. In biomineralization, these heterogeneous nucleators include particles, fibers, and membranes constructed from (macro)molecules of the organic matrix, phospholipid bylayers with associated macromolecules that delimit the mineralization site, and the surface of any precursors present.[29,30] A good example of the intricate control over crystal orientation by heterogeneous nucleation is the assembly of alternating V and R units on the organic baseplate of the coccolith (see Figure 1b).[2–7,31,32]

The impact of the interface on nucleation density, polymorph, and crystallographic orientation is apparent in studies of self-assembled monolayers (SAMs).[33,34] These early reports attribute rapid nucleation of calcite on carboxylate-terminated alkanethiol-based SAMs to a close match in lattice parameters, but ignore the effect of strain at coherent interfaces.[35] Strain has subsequently been shown to modulate calcite crystal shape during growth.[36] Recently, it has become clear that during oriented nucleation, both sides of the interface cooperatively reorganize.[37] A fundamental limitation of the early experiments is that conclusions were based on observations

https://doi.org/10.1557/mrs.2016.90 Published online by Cambridge University Press

made fairly far into the growth stage. Much detail regarding relative rates of nucleation and subsequent growth rates of nuclei, for instance, in different orientations, is therefore lost, and unambiguous interpretation is challenging.

Microfluidic devices have been used to continuously generate solutions of fixed concentrations and pass them over a functionalized interface where crystals nucleate and grow at a constant supersaturation, while allowing *in situ* observations.[24] Heterogeneous nucleation rates of calcite on SAMs were found to be consistent with the predictions of CNT,[22,23,38] and provide estimates of γ_{net} in the range of ~70–100 mJ/m^2 for polysaccharide- and alkanethiol-functionalized surfaces, thereby establishing a lower bound for the surface energy of calcite. Furthermore, there is a direct relationship between γ_{net} and the free energy of binding between calcite and a series of functional groups, consistent with the conventional wisdom that "good binders are good nucleators."[23]

Functional patterning of substrates is thought to be integral to controlling the location of nucleation events, and by extension, hierarchical assembly in biomineralization.[39,40] Looking ahead, such patterning will be essential to improving our understanding of cooperative effects, such as the synergy gained from the presence of both carboxylate and amine-terminated SAMs in the formation of amorphous silica.[41]

Nucleation in confinement

We refer to a system as confined if (a) the phase transformation occurs in one or more small volumes of a supersaturated solution; and (b) transport of at least one building block of the new phase is prevented between these volumes. After division of a bulk system into a large number of small volumes, only a subset will contain suspended nucleators,[41] and phase transformation cannot "spread" from one volume to the next. Ideally, the boundary is a poor heterogeneous nucleator, and the rate converges to that of homogenous nucleation.[41–43]

Phase transformation in confinement will appear to slow down unless very large numbers of droplets are observed. This is because in any system consisting of N identical volumes V_d, with a uniform steady-state intrinsic nucleation rate J_V, the fraction of droplets in which nucleation has occurred is (see the Sear article in this issue):[44]

$$f = 1 - e^{-J_V N V_d t}, \tag{5}$$

where t is the time. The time until nucleation has occurred in 50% of the droplets ($\tau_{1/2}$) is inversely proportional to the number and volume of the droplets (**Figure 2**a–b). In other words, even if the barrier is unchanged, the extrinsic nucleation rate, $J = J_V N V_d$, decreases with decreasing system size.

When confinement approaches the nanoscale, the assumption that nucleation does not affect the composition of the aqueous phase breaks down. For example, if nucleation of an AB solid at some initial σ_i consumes an amount of A and B such that their activities each drop by one-half, the supersaturation is reduced by $\Delta\sigma = \sigma_i - \sigma_f \cong 1.4$, where σ_f is the final supersaturation. Therefore, the particle that just formed is subcritical in size and cannot be the nucleus. This effect is more pronounced in smaller confining volumes for less soluble precipitates and at lower initial supersaturation (Figure 2c).

One can show that at a given σ_i in a confined system of radius r_c, only a particle with radius $r << r_c$ that meets the following equality is in equilibrium after formation:

$$e^{\frac{\gamma V_m}{k_B N_a T}\cdot\frac{1}{r}} + \frac{r^3}{V_m\sqrt{K_{sp}}r_c^3} - e^{\frac{\sigma_i}{2}} = 0, \tag{6}$$

where N_a is Avogadro's number. Below a critical initial supersaturation of σ_i^*, this equation does not have a solution, and nucleation cannot occur. Above σ_i^*, the smaller of the two real solutions corresponds to the nucleus and the larger to the

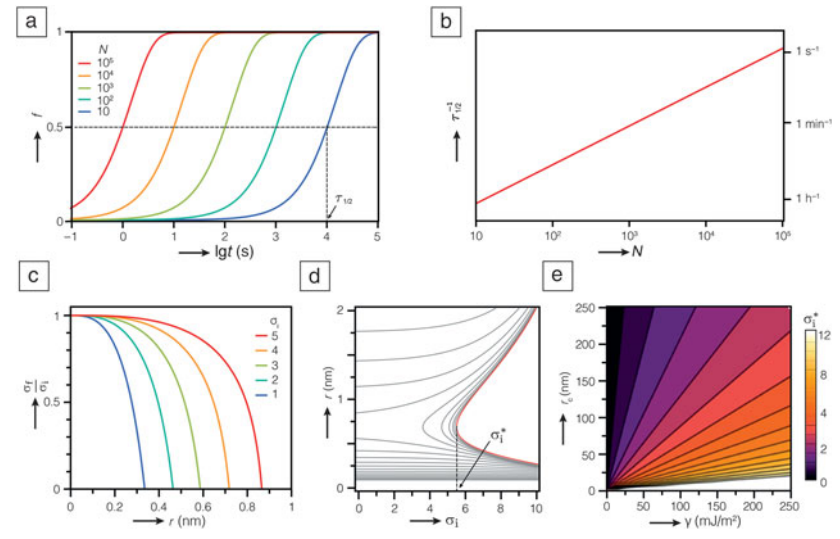


Figure 2. The effect of confinement on nucleation. (a) Plot of the fraction f of N volumes in which nucleation has occurred against log time ($J_V = 10^8$ m^{-3} s^{-1}; $V_d = 65$ pL). (b) Log–log plot of $\tau_{1/2}^{-1}$ versus N, showing the increase in conversion rate with system size. (c–e) Effect of confinement in spherical containers with $r_c = 30$ nm on supersaturation for calcite particles ($K_{sp} = 10^{-8.48}$ M^2, $V_m = 36.9$ cm^3/mol, $\gamma = 0.1$ J/m^2). (c) Fractional drop in supersaturation as a function of particle radius r for initial supersaturation values ranging from 1 to 5. (d) Contour plot of the left-hand side of Equation 6 as a function of the initial supersaturation and the particle radius. The solution of Equation 6 is indicated by the red contour line. (e) Contour plot of the critical supersaturation σ_i^* for nucleation of calcite as a function of the surface free energy and the confining radius. Substantially higher initial supersaturations are required for nucleation as the degree of confinement and the interfacial energy of the nucleus increase. Note: J_V, number of nuclei formed per unit time and unit volume; $\tau_{1/2}$, time until nucleation that has occurred in 50% of the droplets; K_{sp}, solubility product of the new phase; V_m, molar volume of the new phase; γ, surface free energy; σ_i, initial supersaturation; σ_f, final supersaturation; V_d, volume of drop; r_c, confining radius.

https://doi.org/10.1557/mrs.2016.90 Published online by Cambridge University Press

particle in final, stable equilibrium (i.e., the end point of the phase transformation; see Figure 2d–e).

Closely related to the biological systems that inspired them, synthetic liposomes (vesicles bounded by one or more lipid bilayers) have been used to study phase transformations of iron oxides, calcium phosphates, and earth alkaline carbonates in confinement (**Figure 3**a).[51,52] When $CaCO_3$ is precipitated in liposomes between 50 nm and 50 µm in diameter (~130 aL to 130 nL, Figure 3c), ACC forms rapidly, and the supersaturation with respect to calcite is reset to $\sigma = \ln\left[K_{sp}^{ACC} / K_{sp}^{calcite}\right] \approx 4.8$, where K_{sp}^{ACC} is the solubility product of ACC, and $K_{sp}^{calcite}$ is the solubility product of calcite. This increases the nucleation barrier. In sufficiently small liposomes, the supersaturation may even fall below σ_i^*, such that calcite formation becomes impossible. Where nucleation is possible, the time until it is observed in 50 out of 100 liposomes further increases by a factor of 10^4 for the largest liposomes, and a factor of 10^{13} for the smallest liposomes when compared to bulk reaction in 130 mL because of the effect of small volumes on the extrinsic nucleation rate. Taken together, confinement effects dramatically delay the formation of calcite and increase the lifetime of ACC (Figure 3c).[46]

The versatility of confinement effects was demonstrated by the precipitation and transient stabilization (for hundreds of seconds) of a range of amorphous metal carbonates (MCO_3, M = Ca, Sr, Ba, Mn, Cd, Pb) in individually levitated drops with a volume of ~4 µL.[53] Higher throughput was achieved by spray drying from a microfluidic nebulator, where confinement effects, coupled with high supersaturation rates and rapid quenching (drying), resulted in long-term stabilization.[54] Microfluidic devices have also been used to generate surfactant-stabilized microemulsions of aqueous droplets in oil, which offer low polydispersity and improved efficiency of encapsulation compared to liposomes (Figure 3d).[47,55] Confinement further allowed investigating the impact of reagent concentrations on $CaCO_3$ polymorph selectivity and of solubility on nucleation of KNO_3.[56] In the $CaCO_3$ system, confinement in droplets trapped on a patterned SAM (V_d ~ 1 pL, Figure 3e) resulted in a rapid ACC formation, but delayed nucleation of crystalline polymorphs, despite the presence of a relatively powerful nucleating surface.[57]

A range of effects consistent with confinement have also been observed in systems where, unlike in liposomes or droplets, transport of building blocks is possible in at least one direction in space. For example, it has been inferred that the nucleation rate of calcite decreases more rapidly than that of ACC as the diameter of pores in track-etch membranes is reduced from 3 µm to 200 nm (Figure 3f).[49,58] Similar observations were made in the calcium phosphate system.[59] The wedge between a solid half-cylinder resting on a flat

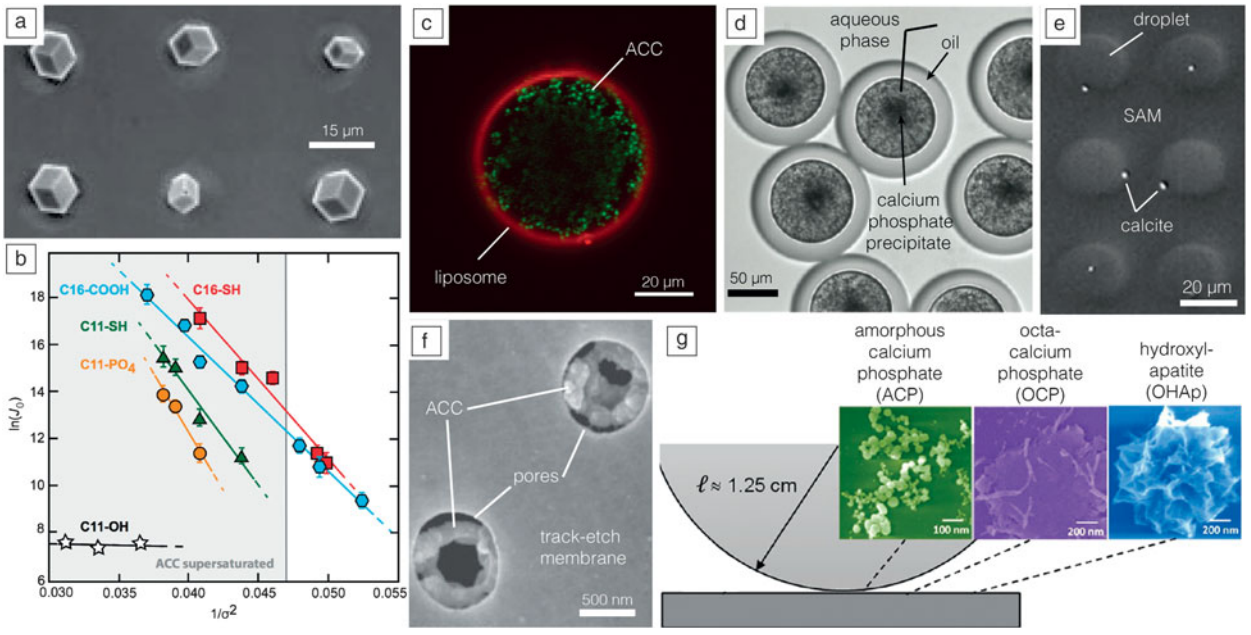


Figure 3. (a) Calcite crystals nucleated on the (001) plane on a self-assembled monolayer (SAM) of $HS(CH_2)_{11}SO_3^-$ supported on Pd.[45] (b) Nucleation rate as a function of (constant) supersaturation for calcite nucleated on SAMs with a range of functional head groups follows predictions of classical nucleation theory, with constant slope proportional to the interfacial energy, γ. Reprinted with permission from Reference 23. © 2014 National Academy of Sciences. (c) Amorphous calcium carbonate (ACC), rather than calcite, precipitates in confinement in giant liposomes, and is stable for long periods of time.[46] (d) Calcium phosphate precipitates formed in double emulsion droplets eventually transform into hydroxylapatite.[47] (e) Calcium carbonate precipitation in aqueous droplets trapped on a patterned SAM results in extended stability of ACC, but eventually, calcite forms; this is likely due to heterogeneous nucleation at the triple line or on the SAM.[48] (f) ACC formed in semiconfining pores (diameter d = 800 nm) in a track-etch membrane.[49] (g) Partial confinement between a cylinder with radius ℓ and a flat substrate resulted in differential stabilization of several metastable intermediates (ACP, OCP, and OHAp) that are typically observed sequentially in hydroxylapatite synthesis.[50] Note: J_0, nucleation rate; σ, supersaturation.

https://doi.org/10.1557/mrs.2016.90 Published online by Cambridge University Press

substrate constitutes a more complex system (Figure 3g), where the degree of confinement can be thought of as rapidly increasing with decreasing distance to the contact line.[48,50,60] Consequently, metastable precursors of crystalline calcium carbonates, sulfates, and phosphates persist for much longer times closer to the contact line. As a result, the "Ostwald–Lussac" sequence of increasingly stable phases observed over time in the bulk system is instead patterned in space. While quantitative treatment of these partially confined systems is more difficult because much depends on geometrical parameters, diffusivities, and mixing, they can be used to rapidly screen for metastable precursors that can be challenging to observe in bulk reactions.

Conclusions

Heterogeneous nucleation and confinement are integral factors to biological control over location, timing, and polymorph selection in biomineralization, but remain challenging to probe quantitatively. This article highlights recent *in vitro* experiments that show how the influence of heterogeneous nucleators can be understood in the context of CNT without needing to invoke "nonclassical" effects. Based on recent experiments and simple thermodynamic considerations, we suggest three ways in which confinement reduces nucleation rates of crystalline biominerals. Amorphous intermediates appear to be less affected. As a result, the lifetime of amorphous precursors can be dramatically longer, even in the absence of any stabilizing additives. This effect may open a window for an organism to manipulate the amorphous material with a low risk of spurious nucleation. Controlled transformation into a crystalline polymorph could then occur by introducing a heterogeneous nucleator into the confined volume, before or after the amorphous intermediate has formed.

References

1. S. Weiner, H.A. Lowenstam, *On Biomineralization* (Oxford University Press, New York, 1989).
2. M.E. Marsh, *Protoplasma* **207**, 54 (1999).
3. M.E. Marsh, A.L. Ridall, P. Azadi, P.J. Duke, *J. Struct. Biol.* **139**, 39 (2002).
4. E.D. Sone, S. Weiner, L. Addadi, *J. Struct. Biol.* **158** (3), 428 (2007).
5. A. Scheffel, M. Gruska, D. Faivre, A. Linaroudis, J.M. Plitzko, D. Schüler, *Nature* **440** (7080), 110 (2005).
6. F. Abreu, A.A. Sousa, M.A. Aronova, Y. Kim, D. Cox, R.D. Leapman, L.R. Andrade, B. Kachar, D.A. Bazylinski, U. Lins, *J. Struct. Biol.* **181** (2), 162 (2013).
7. J. Mahamid, A. Sharir, D. Gur, E. Zelzer, L. Addadi, S. Weiner, *J. Struct. Biol.* **174** (3), 527 (2011).
8. C.T. Hendley, J. Tao, J.A.M.R. Kunitake, J.J. De Yoreo, L.A. Estroff, *MRS Bull.* **40** (6), 480 (2015).
9. C.-M. Wang, H.-G. Liao, F.M. Ross, *MRS Bull.* **40** (1), 46 (2015).
10. W.J.E.M. Habraken, J. Tao, L.J. Brylka, H. Friedrich, L. Bertinetti, A.S. Schenk, A. Verch, V. Dmitrovic, P.H.H. Bomans, P.M. Frederik, J. Laven, P. van der Schoot, B. Aichmayer, G. de With, J.J. DeYoreo, N.A.J. Sommerdijk, *Nat. Commun.* **4**, 1507 (2013).
11. M.H. Nielsen, S. Aloni, J.J. De Yoreo, *Science* **345** (6201), 1158 (2014).
12. F.M. Ross, *Science* **350** (6267), 9886 (2015).
13. A.F. Wallace, L.O. Hedges, A. Fernandez-Martinez, P. Raiteri, J.D. Gale, G.A. Waychunas, S. Whitelam, J.F. Banfield, J.J. De Yoreo, *Science* **341** (6148), 885 (2013).
14. R. Demichelis, P. Raiteri, J.D. Gale, D. Quigley, D. Gebauer, *Nat. Commun.* **2**, 590 (2011).
15. J. Baumgartner, A. Dey, P.H.H. Bomans, C. Le Coadou, P. Fratzl, N.A.J.M. Sommerdijk, D. Faivre, *Nat. Mater.* **12** (4), 310 (2013).
16. J.J. De Yoreo, P.U.P.A. Gilbert, N.A.J.M. Sommerdijk, R.L. Penn, S. Whitelam, D. Joester, H. Zhang, J.D. Rimer, A. Navrotsky, J.F. Banfield, A.F. Wallace, F.M. Michel, F.C. Meldrum, H. Colfen, P.M. Dove, *Science* **349** (6247), aaa6760 (2015).
17. A. Gal, K. Kahil, N. Vidavsky, R.T. DeVol, P.U.P.A. Gilbert, P. Fratzl, S. Weiner, L. Addadi, *Adv. Funct. Mater.* **24** (34), 5420 (2014).
18. A. Navrotsky, *Proc. Natl. Acad. Sci. U.S.A.* **101** (33), 12096 (2004).
19. P.G. Debenedetti, *Metastable Liquids* (Princeton University Press, Princeton, NJ, 1996).
20. J.J. De Yoreo, P.G. Vekilov, *Rev. Mineral. Geochem.* **54**, 57 (2003).
21. R.P. Sear, *J. Phys. Condens. Matter* **19** (3), 033101 (2007).
22. Q. Hu, M.H. Nielsen, C.L. Freeman, L.M. Hamm, J. Tao, J.R.I. Lee, T.Y.J. Han, U. Becker, J.H. Harding, P.M. Dove, J.J. De Yoreo, *Faraday Discuss.* **159**, 509 (2012).
23. L.M. Hamm, A.J. Giuffre, N. Han, J. Tao, D. Wang, J.J. De Yoreo, P.M. Dove, *Proc. Natl. Acad. Sci. U.S.A.* **111** (4), 1304 (2014).
24. T.Z. Forbes, A.V. Radha, A. Navrotsky, *Geochim. Cosmochim. Acta* **75** (24), 7893 (2011).
25. M. Bruno, F.R. Massaro, L. Pastero, E. Costa, M. Rubbo, M. Prencipe, D. Aquilano, *Cryst. Growth Des.* **13** (3), 1170 (2013).
26. W. Sun, S. Jayaraman, W. Chen, K.A. Persson, G. Ceder, *Proc. Natl. Acad. Sci. U.S.A.* **112** (20), E2735 (2015).
27. O. Sohnel, J.W. Mullin, *J. Cryst. Growth* **60**, 239 (1982).
28. D. Gebauer, H. Cölfen, *Nano Today* **6** (6), 564 (2011).
29. N.A.J.M. Sommerdijk, G. de With, *Chem. Rev.* **108** (11), 4499 (2008).
30. F.C. Meldrum, H. Cölfen, *Chem. Rev.* **108** (11), 4332 (2008).
31. F. Nudelman, A.J. Lausch, N.A.J.M. Sommerdijk, E.D. Sone, *J. Struct. Biol.* **183** (2), 258 (2013).
32. F. Nudelman, *Semin. Cell Dev. Biol.* **46**, 1 (2015).
33. J. Aizenberg, *Bell Labs Tech. J.* **10** (3), 129 (2005).
34. J.C. Love, L.A. Estroff, J.K. Kriebel, R.G. Nuzzo, G.M. Whitesides, *Chem. Rev.* **105** (4), 1103 (2005).
35. D. Turnbull, B. Vonnegut, *Ind. Eng. Chem.* **44**, 1292 (1952).
36. B. Pokroy, J. Aizenberg, *CrystEngComm.* **9**, 1219 (2007).
37. D. Quigley, P.M. Rodger, C.L. Freeman, J.H. Harding, D.M. Duffy, *J. Chem. Phys.* **131** (9), 094703 (2009).
38. A.J. Giuffre, L.M. Hamm, N. Han, J.J. De Yoreo, P.M. Dove, *Proc. Natl. Acad. Sci. U.S.A.* **110** (23), 9261 (2013).
39. J. Aizenberg, *Science* **299**, 1 (2003).
40. X. Gong, Y.-W. Wang, J. Ihli, Y.-Y. Kim, S. Li, R. Walshaw, L. Chen, F.C. Meldrum, *Adv. Mater.* **27** (45), 7395 (2015).
41. D. Turnbull, *J. Appl. Phys.* **21** (10), 1022 (1950).
42. Y. Miyazawa, G.M. Pound, *J. Cryst. Growth* **23**, 45 (1974).
43. R.P. Sear, *Int. Mater. Rev.* **57** (6), 328 (2012).
44. R.P. Sear, *CrystEngComm* **16** (29), 6506 (2014).
45. J. Aizenberg, G.M. Whitesides, A.J. Black, *Nature* **398**, 495 (1999).
46. C.C. Tester, M.L. Whittaker, D. Joester, *Chem. Commun.* **50** (42), 5619 (2014).
47. H.C. Shum, A. Bandyopadhyay, S. Bose, D.A. Weitz, *Chem. Mater.* **21** (22), 5548 (2009).
48. C.J. Stephens, S.F. Ladden, F.C. Meldrum, H.K. Christenson, *Adv. Funct. Mater.* **20** (13), 2108 (2010).
49. E. Loste, R.J. Park, J. Warren, F.C. Meldrum, *Adv. Funct. Mater.* **14** (12), 1211 (2004).
50. Y.-W. Wang, H.K. Christenson, F.C. Meldrum, *Chem. Mater.* **26** (20), 5830 (2014).
51. S. Mann, J.P. Hannington, R.J.P. Williams, *Nature* **324**, 565 (1986).
52. J. Collier, P.B. Messersmith, *Annu. Rev. Mater. Res.* **31**, 237 (2001).
53. S.E. Wolf, L. Müller, R. Barrea, C.J. Kampf, J. Leiterer, U. Panne, T. Hoffman, F. Emmerling, W. Tremel, *Nanoscale* **3** (3), 1158 (2011).
54. E. Amstad, M. Gopinadhan, C. Holtze, C.O. Osuji, M.P. Brenner, F. Spaepen, D. Weitz A. *Science* **349** (6251), 956 (2015).
55. M.B. Romanowsky, A.R. Abate, A. Rotem, C. Holtze, D.A. Weitz, *Lab Chip* **12** (4), 802 (2012).
56. P. Laval, A. Crombez, J.-B. Salmon, *Langmuir* **25** (3), 1836 (2009).
57. C.J. Stephens, Y.-Y. Kim, S.D. Evans, F.C. Meldrum, H.K. Christenson, *J. Am. Chem. Soc.* **133** (14), 5210 (2011).
58. A.S. Schenk, E.J. Albarracin, Y.-Y. Kim, J. Ihli, F.C. Meldrum, *Chem. Commun.* **50** (36), 4729 (2014).
59. B. Cantaert, E. Beniash, F.C. Meldrum, *Chem. Eur. J.* **19** (44), 14918 (2013).
60. Y.-W. Wang, H.K. Christenson, F.C. Meldrum, *Adv. Funct. Mater.* **23** (45), 5615 (2013). □

https://doi.org/10.1557/mrs.2016.90 Published online by Cambridge University Press